

# Plasma-assisted atomic layer deposition of highly conductive HfN<sub>x</sub> layers

Saurabh Karwal<sup>1</sup>, Marcel A. Verheijen<sup>1,2</sup>, Wilhelmus M.M. Kessels<sup>1</sup>, [Mariadriana Creatore<sup>1</sup>](#)

<sup>1</sup>*Department of Applied Physics, University of Technology Eindhoven, 5600MB, P.O. Box 513, Eindhoven, Netherlands*

<sup>2</sup>*Philips Innovation labs, High Tech Campus 11, 5656 AE Eindhoven, The Netherlands*

**Abstract:** In this work, we report on the plasma-assisted atomic layer deposition of HfN<sub>x</sub> thin films by employing CpHf(NMe<sub>2</sub>)<sub>3</sub> as the Hf(IV) precursor and Ar-H<sub>2</sub> plasma in combination with external rf substrate biasing as the reducing co-reactant. We show that an increase in the average ion energy up to 304 eV leads to a very low electrical resistivity of  $4.1 \cdot 10^{-4} \Omega\text{cm}$ . This resistivity value is achieved for films as thin as ~35 nm, and it is the lowest resistivity reported in the literature for HfN<sub>x</sub> films grown by either CVD or ALD, while being comparable to the resistivity of PVD-grown HfN<sub>x</sub> films.

**Keywords:** atomic layer deposition, hafnium nitride, rf substrate bias

## 1. Introduction

Conductive transition metal nitride (TMN) films find many applications in nano-electronics. They are used as metal electrodes in metal oxide semiconductor field effect transistors (MOSFETs), and as diffusion barriers in interconnects. In view of the continuous scaling of semiconductor devices, the application of TMN films at increasing small dimensions requires ultra-thin films with low resistivity, besides forming stable interfaces, e.g. with the underlying high-k HfO<sub>2</sub>. Specifically, thin films of titanium nitride and tantalum nitride tend to form undesirable oxy-nitrides at the interface with the HfO<sub>2</sub>. Low resistivity hafnium nitride (HfN) can serve as an effective alternative because of its superior stability when used in combination with HfO<sub>2</sub>. HfN<sub>x</sub> predominantly exists in two crystal phases: highly resistive Hf<sub>3</sub>N<sub>4</sub> with Hf(IV) oxidation state, and low resistivity δ-HfN with Hf(III) oxidation state. The control of the oxidation state of Hf is therefore essential to synthesize conductive HfN<sub>x</sub> layers. Physical vapor deposition (PVD) methods have been widely adopted for the synthesis of low resistivity HfN<sub>x</sub> films. Seo *et al.* have reported the growth of stoichiometric and epitaxial 500 nm thick HfN<sub>x</sub> layers with a resistivity of  $1.4 \cdot 10^{-5} \Omega\text{cm}$ , which is the lowest resistivity reported thus far [1]. On the other hand, the growth of low resistivity HfN<sub>x</sub> films by techniques employing a metal-organic precursor, such as chemical vapor deposition (CVD) or atomic layer deposition (ALD), is very challenging. One of the major challenge is the reduction of Hf(IV) oxidation state in the precursor to Hf(III) oxidation state in the deposited film, as highlighted in our previous work [2]. The urgent requirement from the field of nanoelectronics is the synthesis of ultra-thin films with precise control over film thickness, excellent uniformity and conformality on high aspect ratio 3D nanostructures. These requirements motivate the synthesis of low resistivity HfN<sub>x</sub> films by ALD. We have recently shown that conductive δ-HfN phase can be achieved by adopting CpHf(NMe<sub>2</sub>)<sub>3</sub> as Hf(IV) precursor and H<sub>2</sub> plasma as reducing co-reactant [2]. We demonstrated that the application of an external rf substrate bias during the H<sub>2</sub> plasma step and an increase in the time-averaged substrate potential ( $|V_{\text{bias}}|$ ) from 0V to 130V resulted in a major decrease in electrical resistivity ( $\rho_e$ ) from  $0.9 \Omega\text{cm}$  to  $3.3 \cdot 10^{-3} \Omega\text{cm}$  [3]. The decrease in  $\rho_e$  was found to correlate with a major increase in the fraction of

Hf(III) oxidation state from  $0.65 \pm 0.02$  to  $0.82 \pm 0.02$ . These results demonstrated that the impingement of energetic ions can significantly improve the chemical and electrical properties of HfN<sub>x</sub> thin films prepared by ALD. In the present work, we investigate the effect of Ar-H<sub>2</sub> plasma in combination with external rf substrate biasing during the plasma half cycle as the reducing co-reactant. The impact of impingement of ions with larger mass and higher energy on the chemical and microstructural properties of HfN<sub>x</sub> films is then addressed. We found that an increase in the ion energy up to 304 eV leads to a very low electrical resistivity of  $4.1 \cdot 10^{-4} \Omega\text{cm}$ . To best of our knowledge, this value represents the lowest resistivity reported in the literature for HfN<sub>x</sub> films grown by either CVD or ALD, and is comparable to the resistivity of PVD grown films. Furthermore, this low resistivity is achieved for films as thin as ~35 nm. As will be shown, the HfN<sub>x</sub> films exhibited a high Hf(III) fraction of  $0.86 \pm 0.02$ , comparable to the previously reported H<sub>2</sub> plasma case. In addition, the microstructural characterization revealed that the impingement of ions with a larger mass and higher energy led to a major suppression of the in-grain nano-porosity in the films, key to obtaining the low resistivity HfN<sub>x</sub> layers.

## 2. Experimental

The process was carried out in an Oxford Instruments FlexAL ALD reactor, equipped with an inductively coupled remote plasma (ICP) source with an alumina dielectric tube. A stage temperature of 450°C was selected. This corresponds to a substrate temperature of ~340°C as determined by spectroscopic ellipsometry (SE). The reactor walls were kept at 145°C during all the depositions. The Hf precursor CpHf(NMe<sub>2</sub>)<sub>3</sub> (Air Liquide, >99.99% purity) was contained in a stainless steel bubbler at 60°C and bubbled by an Ar flow of 100 sccm. For the plasma exposure half cycle, an Ar+H<sub>2</sub> gas mixture (10 sccm Ar and 40 sccm H<sub>2</sub>) was introduced into the chamber from the ICP alumina tube. After stabilization of the gas flows for 4 s, the plasma was ignited with 100W radio frequency (rf) ICP power (13.56 MHz) for the desired time. A CpHf(NMe<sub>2</sub>)<sub>3</sub> pulse length of 4 s and plasma exposure of 10 s were used, while keeping the purge step of 2 s after every half cycle. An external substrate bias was applied during the plasma half cycle for the last 5 s using a rf power source (13.56 MHz), attached to the substrate table. The ion flux-energy

distribution functions (IFEDFs) of incident ions were measured using an Impedans Sesion retarding field energy analyzer (RFEA). As reported by Profijt et al. [4], a mono-modal IFEDF for the grounded electrode ( $|V_{\text{bias}}| = 0\text{V}$ ) condition, whereas the application of external rf substrate bias resulted in a bi-modal IFEDF. Furthermore, the RFEA was also used to estimate the flux of incident ions using  $\Gamma_i$ . Films were deposited on planar Si(100) substrates with a diameter of 100 mm and with 450 nm  $\text{SiO}_2$  atop. The growth per cycle (GPC) and the dielectric functions of the  $\text{HfN}_x$  films were examined using spectroscopic ellipsometry (SE, J.A. Woollam, Inc., M2000U). The dielectric functions ( $0.75 \leq h\nu \leq 5.0$  eV) of  $\text{HfN}_x$  films could be modelled using one Drude and two Lorentz oscillators. Additionally, the optical film resistivity ( $\rho_{\text{op}}$ ) was deduced from the free-carrier Drude parameterization. The electrical resistivity ( $\rho_e$ ) was obtained via the four-point probe measurements using a Keithley 2400 SourceMeter and a Signaton probe by multiplying the sheet resistance of the  $\text{HfN}_x$  films with the film thickness as derived from SE. X-ray photoelectron spectroscopy (XPS) measurements were performed using a ThermoScientific KAlpha KA1066 system equipped with a monochromatic Al  $K\alpha$  ( $h\nu = 1486.6$  eV) source in order to study the chemical bonding and the oxidation states of elements present in the film. The chemical composition and the mass density of the films was evaluated via Rutherford backscattering spectrometry (RBS) and elastic recoil detection (ERD) using 1900 keV  $4\text{He}^+$  ions (Detect99). For the ERD measurements, the recoil angle was  $30^\circ$  and the angle of incidence with the sample surface was kept at  $15^\circ$  whereas for the RBS, two detectors were used with scattering angles of  $170^\circ$  and  $150^\circ$ . The surface morphology and the lateral grain sizes of thick  $\text{HfN}_x$  films ( $t > 30$  nm) were studied using a Zeiss Sigma field emission scanning electron microscopy (FESEM) operated at an acceleration voltage of 2 kV. The crystallinity of the  $\text{HfN}_x$  films was examined with a PANalytical X'pert PRO MRD X-ray diffractometer using a Cu  $K\alpha$  ( $\lambda = 1.542$  Å) X-ray source. High angle annular dark-field scanning transmission electron microscopy (HAADF-STEM) studies were conducted using a JEOL ARM 200F operated at 200kV in order to analyze: 1) the lateral grain sizes of thin  $\text{HfN}_x$  films ( $t \leq 10$  nm), defined by the low atomic density grain boundary regions in the top-view images and 2) the microstructure and the nano-porosity of thick  $\text{HfN}_x$  films ( $t > 30$  nm), obtained from the cross-sectional samples. These cross-sectional samples were prepared using a Focused Ion Beam (FIB), following a standard lift-out sample preparation procedure. Prior to FIB milling, a protective layer was deposited on the  $\text{HfN}_x$  layers.  $\text{H}_2$  plasma sample, only EBID Pt/C and IBID Pt was used, as can be recognized from the TEM images below.

### 3. Results

**Ion energy characterization.** The IFEDs for both Ar- $\text{H}_2$  and  $\text{H}_2$ - fed plasmas are presented in Figure 1. The energy distribution of ions with a specific mass cannot

be resolved using RFEA and rather a cumulative distribution of all the ions impinging on the surface is obtained. However, it can be expected that the former plasma contains  $\text{ArH}^+$ ,  $\text{Ar}^+$ ,  $\text{H}_3^+$ ,  $\text{H}_2^+$  and  $\text{H}^+$  ions, with  $\text{ArH}^+$  being the most abundant ion. In a pure  $\text{H}_2$  plasma discharge,  $\text{H}_3^+$  is the most abundant ion. In Figure 1a, a mono-modal IFEDF with an average ion energy ( $E_{\text{ion}}$ ) of 24 eV was obtained for the grounded electrode. When the value of  $|V_{\text{bias}}|$  increased to 246V, the  $E_{\text{ion}}$  increased to 308 eV. Figure 1b shows a similar trend for the case of  $\text{H}_2$  plasma. Next, the flux of impinging ions ( $\Gamma_i$ ) was calculated from the total ion current ( $I_c$ ) recorded by the RFEA. In our case, a constant  $\Gamma_i$  of  $(9.0 \pm 2.1) \cdot 10^{14} \text{ cm}^{-2} \text{ s}^{-1}$  was calculated, independent of  $|V_{\text{bias}}|$  for the Ar/ $\text{H}_2$  plasma, whereas a slight increase in  $\Gamma_i$  from  $(3.1 \pm 0.7) \cdot 10^{14} \text{ cm}^{-2} \text{ s}^{-1}$  at  $|V_{\text{bias}}| = 0\text{V}$  to  $(9.5 \pm 2.2) \cdot 10^{14} \text{ cm}^{-2} \text{ s}^{-1}$  at  $|V_{\text{bias}}| = 173\text{V}$  was observed for the  $\text{H}_2$  plasma process. Based on these results, we concluded that the values of  $\Gamma_i$  for both the processes were relatively similar in the entire range of  $|V_{\text{bias}}|$  investigated, whereas a significant increase in  $E_{\text{ion}}$  occurred.

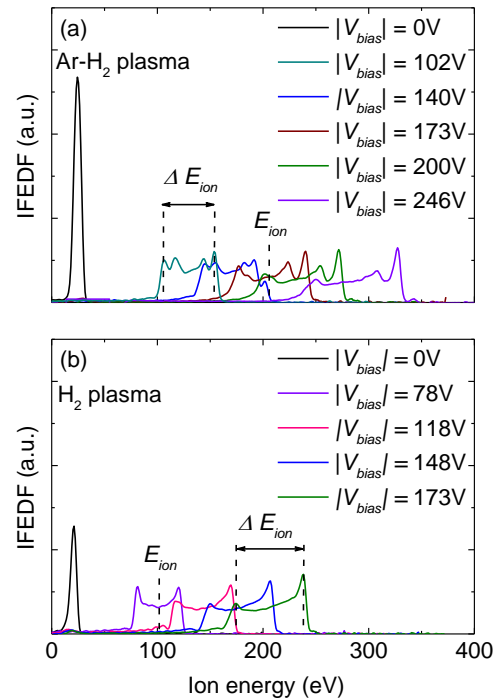


**Figure 1.** Ion flux-energy distribution functions (IFEDFs) for ions in a (a) Ar- $\text{H}_2$  plasma operated at 6 mTorr and (b)  $\text{H}_2$  plasma operated at 30 mTorr for various values of  $|V_{\text{bias}}|$ .

**$\text{HfN}_x$  opto-electrical properties.** The GPC was found to be constant at  $0.35 \pm 0.04$  Å/cycle, independent of the increase in  $|V_{\text{bias}}|$ . Figure 2a shows the  $\rho_e$  and the  $\rho_{\text{op}}$  values for  $\text{HfN}_x$  films as a function of  $|V_{\text{bias}}|$ . The  $\text{HfN}_x$  films grown at  $|V_{\text{bias}}| = 0\text{V}$  using an Ar- $\text{H}_2$  plasma exhibit a high  $\rho_e$  of  $(2.0 \pm 0.1) \cdot 10^{-1} \Omega\text{cm}$  and a low  $\rho_{\text{op}} = (5.2 \pm 0.1) \cdot 10^{-3} \Omega\text{cm}$ . When increasing the  $|V_{\text{bias}}|$  value

up to 255V, a substantial decrease in  $\rho_e$  to  $(4.1 \pm 0.1) \cdot 10^{-4} \Omega\text{cm}$  and in  $\rho_{op}$  to  $(2.4 \pm 0.1) \cdot 10^{-4} \Omega\text{cm}$  was observed. Figure 2a also contains the previously reported  $\rho_e$  and  $\rho_{op}$  data for the  $\text{H}_2$  plasma process for comparison [3]. It should be noted that the very low  $\rho_e$  achieved at  $|V_{bias}| = 255\text{V}$  is for  $\text{HfN}_x$  films as thin as  $\sim 35\text{ nm}$ . This resistivity value is the lowest ever for the  $\text{HfN}_x$  films grown by either CVD or ALD, and is comparable to the films grown by PVD. The  $|V_{bias}|$  value that yields the minimum in  $\rho_e$  and  $\rho_{op}$  values is referred to as optimum condition for the corresponding ALD process and the rest of the manuscript will address the film characterization only at the optimum conditions. By considering that the interaction distance of the incident light with the  $\text{HfN}_x$  films is rather small, it can be expected that only the crystalline quality within 3-4 nm is probed by SE for determining the  $\rho_{op}$ . Therefore, the difference between  $\rho_e$  and  $\rho_{op}$  ( $\Delta\rho$ ) provides insights into the amount of electronic scattering in  $\text{HfN}_x$  films. Specifically, the application of Ar/ $\text{H}_2$  plasma greatly reduced the amount of electronic scattering in  $\text{HfN}_x$ .

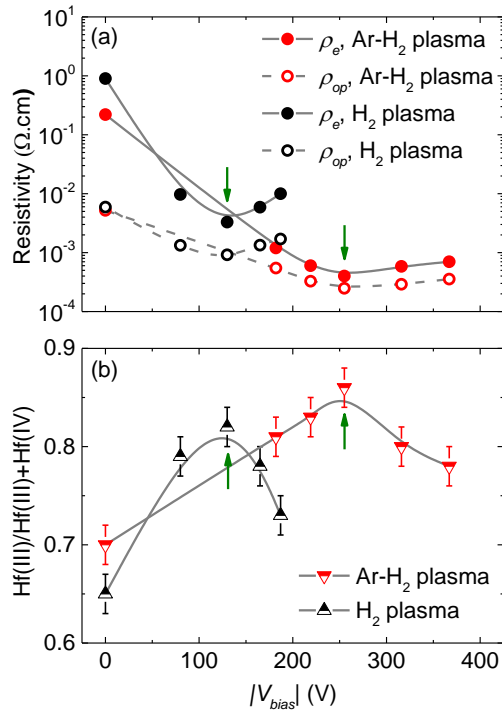


**Figure 2.** (a) Electrical ( $\rho_e$ ) and optical resistivity ( $\rho_{op}$ ) values for  $\sim 35\text{ nm}$   $\text{HfN}_x$  films grown using Ar- $\text{H}_2$  plasma compared with  $\sim 80\text{ nm}$   $\text{HfN}_x$  films grown using  $\text{H}_2$  plasma and (b) the corresponding Hf(III) oxidation state fractions as a function of  $|V_{bias}|$ . Lines serve as a guide to the eye and the green arrows indicate the *optimum condition* in terms of minimum in resistivity achieved in both ALD processes.

**HfN<sub>x</sub> chemical composition.** Figure 2b shows the Hf(III) oxidation state fraction as a function of  $|V_{bias}|$ . For comparison, the previously reported Hf(III) fraction data

for  $\text{H}_2$  plasma is also shown. The Hf(III) fraction increased from  $0.70 \pm 0.02$  to  $0.86 \pm 0.02$  upon increasing the  $|V_{bias}|$  from 0V up to the optimum condition. Interestingly, the high Hf(III) fraction achieved at the optimum condition for Ar/ $\text{H}_2$  plasma is comparable to the previously reported  $\text{H}_2$  plasma (i.e.  $0.86 \pm 0.02$  vs.  $0.82 \pm 0.02$ ). The aforementioned increase in Hf(III) fraction upon increasing the  $|V_{bias}|$  from 0V to 255V is correlated with a major decrease in O content from  $19.9 \pm 0.9\text{ at.}\%$  to  $<2\%$ .

**HfN<sub>x</sub> microstructural properties.** Conducting  $\delta$ -HfN phase was observed for the *optimum condition* of the Ar- $\text{H}_2$  plasma, exhibiting HfN(111), HfN(200) and HfN(220) reflections in a similar peak intensity ratio as the powder  $\delta$ -HfN pattern, indicating no preferred growth direction. The lateral grain sizes of the  $\text{HfN}_x$  films were subsequently investigated by means of top-view high-angle annular dark-field scanning transmission electron microscopy (HAADF-STEM) and scanning electron microscopy (SEM) images (not reported here). It was concluded that the rate of lateral grain growth was higher for Ar- $\text{H}_2$  plasma as compared to the  $\text{H}_2$  plasma (Figure 3).

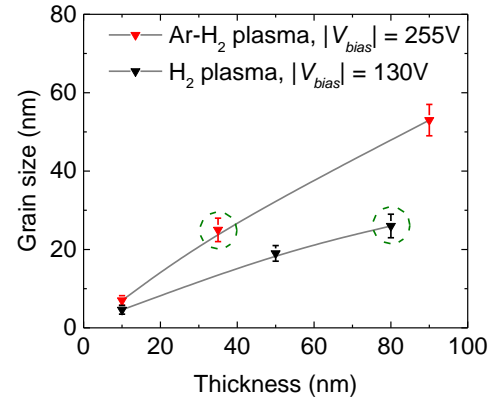


**Figure 3.** Lateral grain sizes for the  $\text{HfN}_x$  films prepared at the *optimum conditions* of the Ar- $\text{H}_2$  plasma and  $\text{H}_2$  plasma as a function of film thickness. The points with the green circle indicates the grain sizes of  $\text{HfN}_x$  films that are discussed in terms of resistivity for the corresponding ALD process.

Figure 4 shows the HAADF-STEM image of cross-sectional samples for the Ar- $\text{H}_2$  plasma and the  $\text{H}_2$  plasma. Dark regions in the films indicate the presence of lighter elements and/or porosity. The images with a 50 nm scale display the lateral development of crystal grains as a function of height, yielding similar grain size values on the top surfaces of the film as reported in Figure 3. The higher magnification insets reveal that the  $\text{HfN}_x$  film grown using Ar- $\text{H}_2$  plasma are quite dense. On the other hand, non-uniform contrast variations and dark patches can be observed within the crystal grains of the  $\text{HfN}_x$  film grown using  $\text{H}_2$  plasma, suggesting the presence of lower density regions, such as nano-pores. In addition, we observed the

presence of V-shaped pyramidal void for the Ar-H<sub>2</sub> plasma in the initial phase of film growth (Figure 4a). The cause for this phenomenon is not known yet. Although the voids can be observed in several areas of the whole TEM cross-section of the Ar/H<sub>2</sub> sample (data not shown), it appears that their presence does not affect the film electrical properties. This suggests that charges can be transported through the dense regions of the layer.

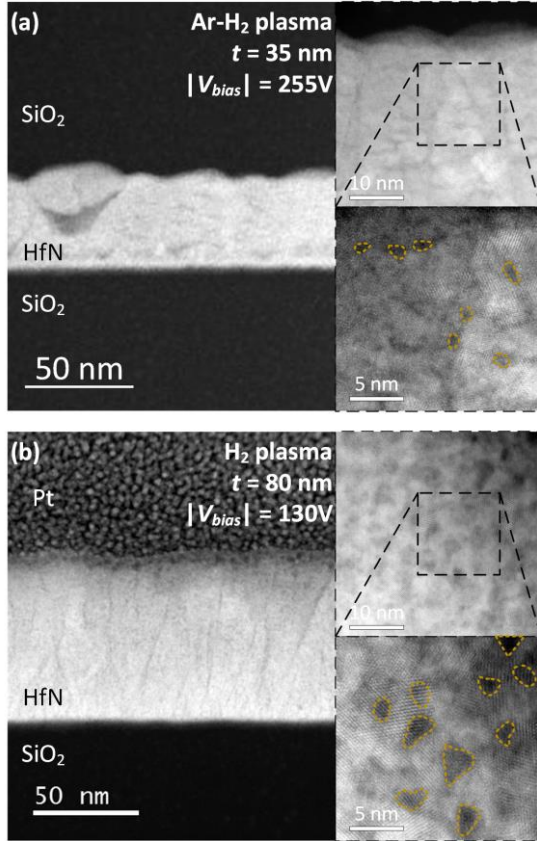


Figure 4. Cross-sectional high-angle annular dark-field scanning transmission electron microscopy (HAADF-STEM) images for (a) ~35 nm thick film grown at  $|V_{bias}| = 255V$  using Ar-H<sub>2</sub> plasma and (b) ~80 nm thick film prepared using H<sub>2</sub> plasma at  $|V_{bias}| = 130V$ . The insets show magnified views of the microstructure displaying the nano-scale porosity in the film as indicated by yellow areas.

#### 4. Discussion and Conclusions

Plasma-assisted ALD of HfN<sub>x</sub> has been reported using CpHf(NMe<sub>2</sub>)<sub>3</sub> as Hf(IV) precursor and Ar/H<sub>2</sub> plasma in combination with an external rf substrate bias application as reducing co-reactant. From the ion energy characterization, it is concluded that the energy of the impinging ions on the HfN<sub>x</sub> surface at the optimum condition of Ar/H<sub>2</sub> plasma ( $E_{ion} = 304$  eV) is significantly higher than for the H<sub>2</sub> plasma ( $E_{ion} = 159$  eV). On the other hand, the  $I_i$  at the optimum conditions for Ar/H<sub>2</sub> plasma and H<sub>2</sub> plasma are comparable. Furthermore, it is also safe to conclude that the HfN<sub>x</sub> film surface is subjected to impingement of ions with a larger mass

using Ar/H<sub>2</sub> plasma than in the case of H<sub>2</sub> plasma. A very low  $\rho_e$  of  $4.1 \cdot 10^{-4} \Omega cm$  is achieved for films under Ar/H<sub>2</sub> plasma condition, and as thin as ~35 nm. Based on the extensive thin film characterization, it is concluded that the chemical composition and the lateral grain size of ~35 nm thick HfN<sub>x</sub> films grown using Ar/H<sub>2</sub> plasma are comparable to the previously reported ~80 nm thick films grown using H<sub>2</sub> plasma. Therefore, the very low  $\rho_e$  in the case of Ar-H<sub>2</sub> plasma is the result of a major suppression of the in-grain nano-porosity. This conclusion agrees with the aforementioned observation on the much lower electronic scattering (i.e.  $\Delta\rho$ ) for the case of Ar/H<sub>2</sub> plasma (Figure 2a), resulting from the higher in-grain crystal quality. It is suggested that the impinging ions with a higher energy and larger mass may deliver a more efficient energy and momentum transfer to the HfN<sub>x</sub> film surface. The enhanced energy and momentum transfer may facilitate near-surface and sub-surface diffusion processes, having a role in annihilating defects, such as nano-porosity. The obtained results demonstrate how energy and mass of impinging ions during plasma ALD can contribute to the fine tuning of the chemical and microstructural properties of HfN<sub>x</sub> thin films and may be applicable to wide range of ALD processes for the growth of other transition metal nitrides.

#### 5. References

- [1] Seo, H. S. et al., J Appl Phys 96, 878, (2004).
- [2] Karwal, S. et al., J. Vac. Sci. Technol. A Vac. Surf. Films 35, 01B129 (2017).
- [3] Karwal, S. et al., Journal of Materials Chemistry C 6, 3917 (2018).
- [4] Profijt, H. B., et al., J. Vac. Sci. Technol. A 31, 01A106 (2013).